

Modeling and Identification of a 3-DOF Planar Actuator with Manipulator*

Michal Gajdušek, Ad Damen, Paul v.d. Bosch

Department of Electrical Engineering, Eindhoven University of Technology,
The Netherlands, (Tel:+31-(0)40-247-3142; e-mail: m.gajdusek@tue.nl)

Abstract: The goal of this paper is to describe the identification and modeling of a 3-degree-of-freedom (DOF) platform with a manipulator on top of it, which is magnetically levitated by 9 voice-coil actuators. This 3-DOF experimental setup is a pre-prototype of a 6-DOF magnetically levitated platform with manipulator in order to study combined control of both the platform and manipulator.

1. INTRODUCTION

In lithography industry or for pick-and-place machines there is a tendency to increase precision of production at high speeds. In lithography industry wafers are processed with precision in nanometer scale, but the position must be changed very fast to reduce processing time. These two requirements lead to design of a new generation of vibration-free manipulators based on magnetic levitation and propulsion. Such manipulators can work in vacuum and if we combine such a magnetically levitated and propelled planar actuator with a precise manipulator on top of it, we can achieve a high-precision, high-speed, vibration-free manipulator. Control of magnetically levitated contactless planar actuator with 6 DOFs is itself difficult task (e.g. van Lierop *et al.*, 2006; Ueda and Ohsaki, 2007; Compter, 2004). An even bigger challenge is to control such a planar actuator with an added manipulator on top of it. The manipulator causes disturbing forces and torques acting on the platform. The goal of this paper is to describe the modeling and identification of a 3-DOF experimental setup which was build as a pre-prototype of a fully 6-DOF planar actuator with a manipulator on top.

In the final 6-DOF prototype levitation and propulsion will be provided with coils in standstill base-plate together with permanent magnets in the platform, see (van Lierop *et al.*, 2006). The manipulator on the platform will be wirelessly controlled and powered, see (de Boeij *et al.*, 2006). Such wireless system allows for combination of long-stroke movement of the platform with precise short-stroke movement of the manipulator (Fig. 1).

In order to test and validate control design for the final contactless planar actuator with manipulator, an experimental setup has been designed, which yields only 3 DOFs for the platform, see Gajdusek *et al.* (2007). Precise control of the platform is necessary, because in the final prototype the platform will be lifted and operate just about 1 mm or less above the surface. Such a working condition is a trade off between operational height and power needed to lift the platform with the manipulator in the final prototype.

Description of the experimental setup is provided in section 2 of this paper. Section 3 describes a model of the experimental setup. In section 4, the identification procedure and results are presented.

2. EXPERIMENTAL SETUP

The experimental setup consists of two main parts: a 3-DOF platform actuated by 9 voice coils and 2-DOF manipulator on top of it (Fig. 2).

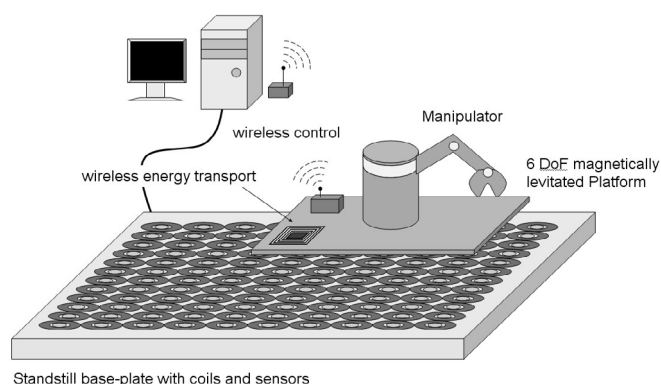


Fig. 1. Concept of 6-DOF magnetically levitated platform with manipulator

* This IOP-EMVT project is funded by SenterNovem. SenterNovem is an agency of the Dutch Ministry of Economical Affairs.

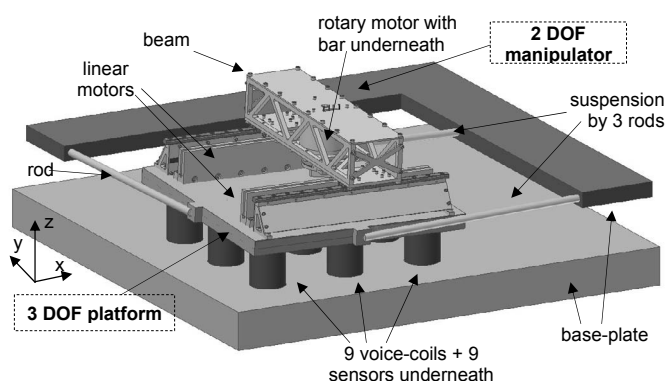


Fig. 2. Drawing of the experimental setup

The platform, that mimics the final magnetic array, is suspended such that it can only move in 3 DOFs: vertically and over two tilting angles. The other 3 DOFs are fixed by a suspension system consisting of 3 rods connecting the platform with the base-plate. Because the final planar actuator will be magnetically levitated and controlled in 6 DOFs in vacuum, it will have zero spring constants and zero damping. Therefore the suspension system was designed in a way to achieve minimal spring constants and minimal damping in 3 DOFs as well, but with very high stiffness in other 3 DOFs. We have chosen the option with built-in leaf-springs at the ends of the rods. The rods can easily bend in two directions at its ends but they cannot shrink or extend, so they behave as a spring with low spring constant in two directions and with high spring constant elsewhere. This feature of the suspension rods was unfortunately also their drawback, as will be shown later.

The platform is actuated by 9 voice coils underneath which are distributed into regular array to simulate the topology of the final planar actuator and is used for gravity compensation and for manipulator platform control in 3 DOFs. Using this over-actuated platform allows us also to distribute necessary force for lifting the platform as well as to control disturbances from the manipulator. The total force produced by nine voice coils is about 180 N. Part of this force will be used for gravity compensation. With a total weight of the platform with manipulator of about 7 kg, the force available for control will be approximately equal to 110 N. Because of the actuators shape, voice coils also behave as air dampers.

Furthermore inductive position sensors are mounted under each voice coil in such a way that we have measurement at the same position as the actuator acts (Fig. 3). Such over-actuated and over-sensed system allows us also to observe and compensate for flexible modes of the platform.

The manipulator on top of the platform is essentially an H-bridge with a rotary motor on the beam. For high stiffness of the manipulator the following design has been chosen. The manipulator consists of two parallel three-phase linear motors with encoders which are connected by stiff beam. In the middle of the beam is a synchronous three-phase rotary motor with encoder (Fig. 4). Together the 3 motors provide precise linear and rotary movement of an end tip of the manipulator.

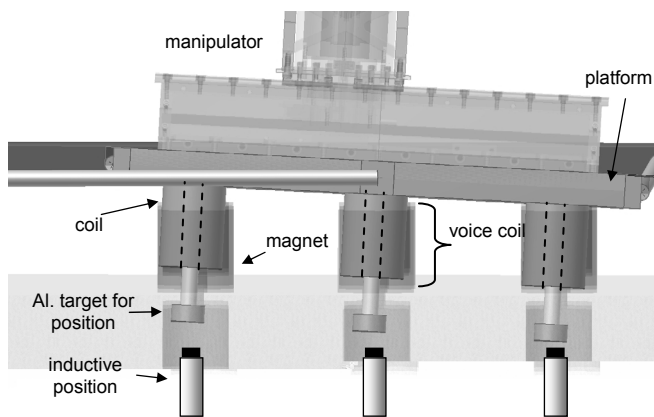


Fig. 3. Drawing of the experimental setup; cross-section

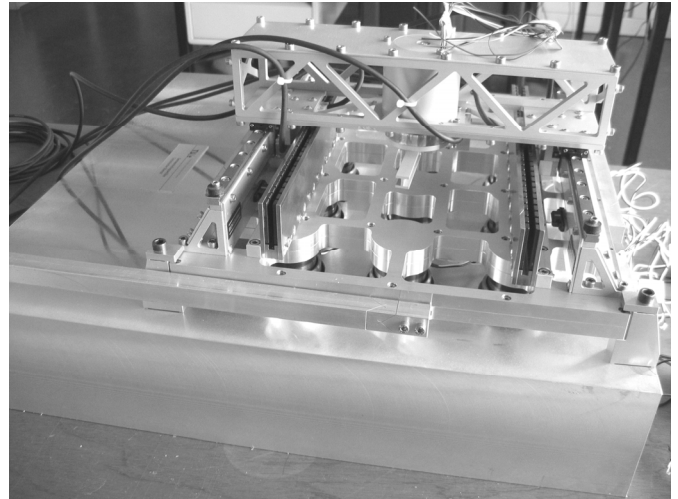


Fig. 4. Photo of the experimental setup

3. MODEL

The model of the whole system consists of two main parts. Equations of motion of the manipulator have been presented in Zuurendonk, *et al.* (2007). Here, the model of the 3-DOF planar actuator (platform) is derived. The model is based on the following assumptions:

We are assuming a rigid body of the platform and manipulator to start with.

The system is assumed to be operating around zero working point where gravitational forces are already counteracted.

The effect of the rotary motor with connected bar is neglected, because it produces significant disturbing torque only around z-axis which is suspended and the effect on controlled DOFs is very small.

Only small deviations around the zero working point are assumed.

Forces and torques due to movement of the manipulator are considered counteracted by the suspension system and by feed-forward. Therefore manipulator interacts with the platform only statically by the change of the mass matrix.

Using these assumptions, we can derive equations of motions only for the platform, where the position of the beam of the manipulator appears as a parameter:

$$\mathbf{M}(x_b)\ddot{\underline{q}} + \mathbf{H}(\underline{q}, \dot{\underline{q}}) = \underline{\tau}, \quad (1)$$

where $\underline{q} = [\psi \ \theta \ z]^T$ is a column of coordinates describing orientations about x- and y-axis, and the vertical position, respectively. Applied wrench (force and torques) column $\underline{\tau} = [T_\psi \ T_\theta \ F_z]^T$ consists of two torques applied about x- and y-axis and force applied in vertical direction. The linearized mass matrix then is:

$$\mathbf{M}(x_b) = \begin{bmatrix} J_\psi + m_b z_b^2 & J_\psi \theta & 0 \\ J_\psi \theta & J_\theta + m_b (z_b^2 + x_b^2) & m_b x_b \\ 0 & m_b x_b & m_p + m_b \end{bmatrix}, \quad (2)$$

where x_b and z_b are relative positions of the beam of the manipulator with respect to the origin O in x - and z -direction (see Fig. 5). m_p and m_b are masses of the platform (together with the static part of the manipulator) and the beam, respectively, and J_ψ , J_θ and $J_\psi \theta$ are moments of inertia of the whole system. The center of mass of the platform is not exactly in the origin of the coordinate system because of weight of the voice coils, attached suspending rods and static part of the manipulator. These terms are also included in the mass matrix, but for simplicity not shown. The linearized joined matrix is given by:

$$\mathbf{H}(\underline{q}, \dot{\underline{q}}) = \begin{bmatrix} \underline{k}_1 \underline{q} - z_b m_b g \psi + 6r_{vc}^2 d \dot{\psi} \\ \underline{k}_2 \underline{q} - z_b m_b g \theta + 6r_{vc}^2 d \dot{\theta} \\ \underline{k}_3 \underline{q} + 9d \dot{z} \end{bmatrix}, \quad (3)$$

where d is damping coefficient of the voice coils, r_{vc} is arm of the voice coils/sensors (see Fig. 6). gravity constant $g = 9.81 \text{ m}\cdot\text{s}^{-2}$, and \underline{k}_1 , \underline{k}_2 and \underline{k}_3 are row vectors containing spring constants derived from the fact that suspending rods behave as a spring with different spring constants in each direction (k_{linear} , $k_{\text{torque_low}}$, and $k_{\text{torque_high}}$). They have been designed to have low spring constant for movement in vertical direction. Unfortunately the rods also twist when the platform is tilted. This causes high torque spring constants for tilting about x - and y -axis (Fig. 7).

The joined matrix can be split into a stiffness matrix

$$\mathbf{K} = \frac{\partial \mathbf{H}}{\partial \underline{q}} = \begin{bmatrix} \underline{k}_1 + [-z_b m_b g \quad 0 \quad 0] \\ \underline{k}_2 + [0 \quad -z_b m_b g \quad 0] \\ \underline{k}_3 \end{bmatrix}, \quad (4)$$

and a damping matrix

$$\mathbf{D} = \frac{\partial \mathbf{H}}{\partial \dot{\underline{q}}} = \begin{bmatrix} 6r_{vc}^2 d & 0 & 0 \\ 0 & 6r_{vc}^2 d & 0 \\ 0 & 0 & 9d \end{bmatrix}. \quad (5)$$

Then $\mathbf{H}(\underline{q}, \dot{\underline{q}}) = \mathbf{K}\underline{q} + \mathbf{D}\dot{\underline{q}}$ and equation of motion (1) can be rewritten as linear parameter-varying (LPV) system:

$$\mathbf{M}(x_b) \ddot{\underline{q}} + \mathbf{D}\dot{\underline{q}} + \mathbf{K}\underline{q} = \underline{\tau}. \quad (6)$$

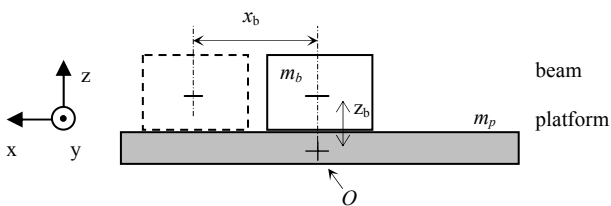


Fig. 5. Drawing of simplified model of the platform with moving beam

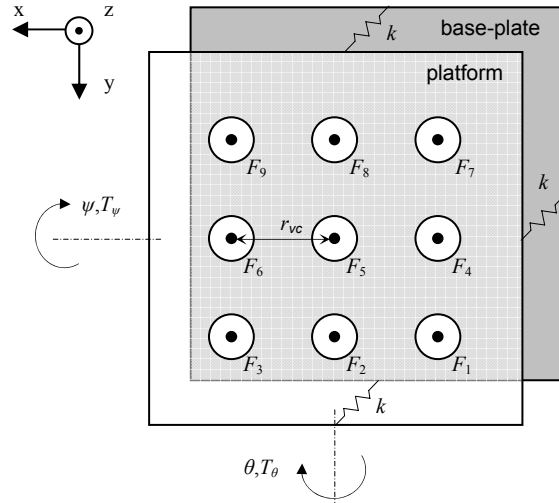


Fig. 6. Distribution of actuators and springs on the platform

We can also describe the system with a state space model:

$$\dot{\underline{x}} = \mathbf{A}(x_b) \underline{x} + \mathbf{B}(x_b) \underline{\tau}, \quad (7)$$

$$\underline{q} = \mathbf{C}\underline{x},$$

where:

$$\mathbf{A}(x_b) = \begin{bmatrix} \mathbf{I} & \mathbf{0} \\ \mathbf{0} & \mathbf{M}(x_b) \end{bmatrix}^{-1} \begin{bmatrix} \mathbf{0} & \mathbf{I} \\ -\mathbf{K} & -\mathbf{D} \end{bmatrix}, \quad (8)$$

$$\mathbf{B}(x_b) = \begin{bmatrix} \mathbf{I} & \mathbf{0} \\ \mathbf{0} & \mathbf{M}(x_b) \end{bmatrix}^{-1} \begin{bmatrix} \mathbf{0} \\ \mathbf{I} \end{bmatrix},$$

$$\mathbf{C} = [\mathbf{I} \quad \mathbf{0}],$$

$$\text{and state vector } \underline{x} = [\underline{q} \quad \dot{\underline{q}}]^T = [\psi \quad \theta \quad z \quad \dot{\psi} \quad \dot{\theta} \quad \dot{z}]^T.$$

It is obvious that the platform is a system with 9 actuators and 9 sensors, but just with 3 DOFs. Therefore we need transformation from $\underline{\tau}$ to the vector \underline{u} of the 9 actuator forces F_{1-9} according to $\underline{u} = \mathbf{T}^T \underline{\tau}$:

$$\mathbf{T} = \begin{bmatrix} 1/6r_{vc} & 0 & -1/6r_{vc} & 1/6r_{vc} & 0 & -1/6r_{vc} & 1/6r_{vc} & 0 & -1/6r_{vc} \\ 1/6r_{vc} & 1/6r_{vc} & 1/6r_{vc} & 0 & 0 & 0 & -1/6r_{vc} & -1/6r_{vc} & -1/6r_{vc} \\ 1/6 & 1/6 & 1/6 & 1/6 & 1/6 & 1/6 & 1/6 & 1/6 & 1/6 \end{bmatrix}. \quad (9)$$

A second transformation is from the vertical position sensors outputs \underline{y} to the column of coordinates $\underline{q} = \mathbf{T}\underline{y}$. These linearized transformation matrices are not unique. They have been chosen to utilize power of the actuators and reduce noise from the sensors.

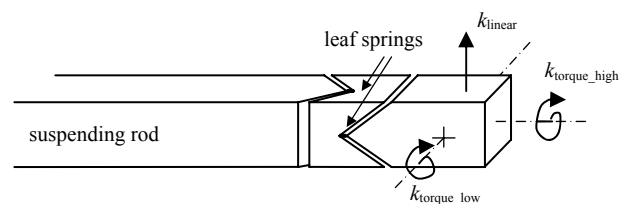


Fig. 7. Suspending rod; linear and torque spring behaviour

4. IDENTIFICATION

Because the planar actuator is an almost meta-stable system (ideally double integration in each DOF), identification should be performed on a closed-loop system. There have been developed many different methods for closed-loop identification in the past. Classical methods are joint input-output identification (e.g. Ng, *et al.*, 1977; Söderström and Stoica, 1989), instrumental variable (Söderström *et al.*, 1987; Gilson and Van den Hof, 2003) or direct identification (Söderström *et al.*, 1976; Ljung, 1993). Recently developed methods are for example two-stage (Van den Hof and Schrama, 1993), identification of coprime factorization (Schrama, 1992; Van den Hof *et al.*, 1995) or dual-Youla parameterization (e.g. Vidyasagar, 1985). We have chosen classical indirect method for closed-loop identification, see (e.g. Gustavsson *et al.*, 1977; Van den Hof and de Callafon, 1996), because the plant itself is nearly unstable and the controller transfer function is known as well as the excitation signal.

Identification of the closed-loop system has been done using two different indirect approaches. In the first approach time-domain data of the system were processed using Ho-Kalman algorithm (Ho and Kalman, 1966). The second approach was based on frequency-domain system identification, where data were obtained from the system using signal and system analyzer *SigLab*.

A controller, consisting of three separate SISO PI controllers, has been used to stabilize the system. So the three DOFs are controlled separately. The integrative components have been used to remove steady-state errors. For each method, the position of the beam x_b - parameter of the system - was set to three different locations: most left, middle and most right.

In the *first approach* of closed-loop identification, transfer function \mathbf{G} from \underline{y} to \underline{y} has been identified (Fig. 8). Gaussian white noise has been applied as a disturbance each time in turn at one of the inputs of the planar actuator. All 3 outputs of the planar actuator have been measured to obtain direct- and cross-transfer functions of \mathbf{G} , where $\mathbf{G} = \mathbf{P}(\mathbf{I}+\mathbf{C}\mathbf{P})^{-1}$. There were performed two experiments with sampling rate of 1 kHz and 10 kHz with about the same results.

From the measured time-domain data, cross-correlation functions from the each input to the each output have been derived. Because the input signal was white noise process, estimating the cross-correlation function directly provides us with information of the pulse response of the system

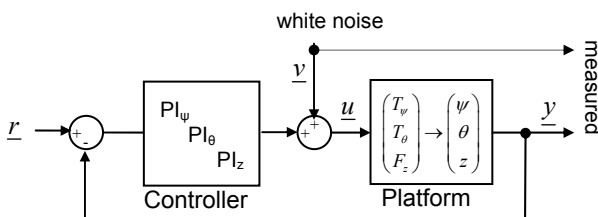


Fig. 8. The closed-loop system with applied white noise

(Oppenheim and Schaffer, 1999). Identified pulse response sequence $\{g(t)\}_{t=0, \dots, \infty}$ was used in Ho-Kalman algorithm as the sequence of *Markov parameters* of the system $G(z) = \sum_{t=0}^{\infty} g(t)z^{-t}$.

The algorithm is based on the Hankel matrix

$$\mathbf{H}(G) = \begin{bmatrix} g(1) & g(2) & g(3) & \dots & g(n_c) \\ g(2) & g(3) & g(4) & \dots & \vdots \\ g(3) & g(4) & g(5) & \dots & \vdots \\ \vdots & \vdots & \vdots & \ddots & \vdots \\ g(n_r) & \dots & \dots & \dots & g(n_c + n_r - 1) \end{bmatrix}, \quad (10)$$

which has the same elements on the skew diagonals. The matrices $(\mathbf{A}_n, \mathbf{B}_n, \mathbf{C}_n, \mathbf{D}_n)$ of estimated state space model \mathbf{G}_n of the system \mathbf{G} , in the form

$$\mathbf{G}_n : x(t+1) = \mathbf{A}_n x(t) + \mathbf{B}_n u(t), \quad y(t) = \mathbf{C}_n x(t) + \mathbf{D}_n u(t), \quad (11)$$

can be constructed applying singular value decomposition on the Hankel matrix (Zeiger and McEwen, 1974)

$$\mathbf{H} = \mathbf{U}_n \mathbf{\Sigma}_n \mathbf{V}_n^T. \quad (12)$$

Then we can derive the matrices of the state space model as

$$\begin{aligned} \mathbf{A}_n &= \mathbf{\Sigma}_n^{-1/2} \mathbf{U}_n^T \cdot \bar{\mathbf{H}} \cdot \mathbf{V}_n \mathbf{\Sigma}_n^{-1/2}, & \mathbf{B}_n &= \mathbf{U}_n \mathbf{\Sigma}_n^{1/2}, \\ \mathbf{C}_n &= \mathbf{\Sigma}_n^{1/2} \mathbf{V}_n^T, & \mathbf{D}_n &= g(0), \end{aligned} \quad (13)$$

where $\bar{\mathbf{H}}$ is the shifted Hankel matrix by one block column to the left. A valuable feature of the Ho-Kalman algorithm is that it can handle also MIMO systems. Thus each $g(i)$ element of the \mathbf{H} represents a $m \times p$ matrix, which corresponds to pulse response of MIMO system with p inputs and m outputs at a time instant t_i . For our 3-DOF system, submatrices have dimensions of 3×3 elements. Reconstructed state-space model consists of states which are common for whole MIMO model. Because the measured data are not exact, it is necessary to reduce order of the model by choosing number of relevant singular values in $\mathbf{\Sigma}_n$ matrix. From magnitude of the singular values (Fig. 9) we have verified that the identified model \mathbf{G}_n has 9 main states, which corresponds to 6 states of the platform with 3 states of the

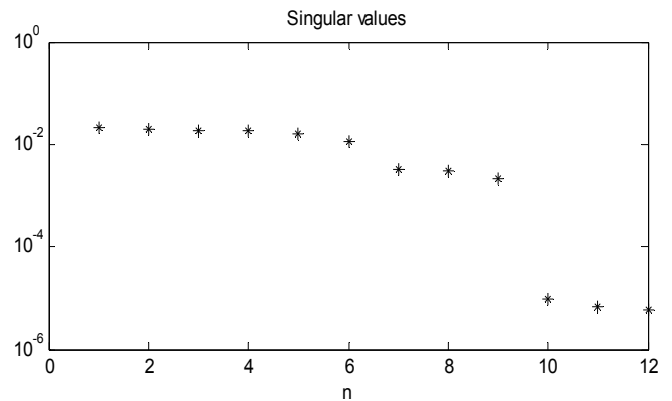


Fig. 9. Largest 12 singular values of the system

controller. Now we want to reconstruct plant transfer functions \mathbf{P}_n from estimate \mathbf{G}_n , by solving the equation $\mathbf{G}_n = \mathbf{P}_n(\mathbf{I} + \mathbf{C}\mathbf{P}_n)^{-1}$. An exact solution of \mathbf{P}_n follows by taking

$$\mathbf{P}_n = \mathbf{G}_n (\mathbf{I} - \mathbf{C}\mathbf{G}_n)^{-1}, \quad (14)$$

which can be calculated as the controller \mathbf{C} is known. Bode magnitude plot of the frequency response of the identified plant \mathbf{P}_n is shown on Fig. 10.

In the *second approach*, frequency-domain data were obtained from the system using signal and system analyzer *SigLab* (from Spectral Dynamics, Inc.). As a source, Gaussian white noise was used again, but the frequency response of the input sensitivity $\hat{\mathbf{S}}(j\omega) = (\mathbf{I} + \mathbf{C}(j\omega)\hat{\mathbf{P}}(j\omega))^{-1}$ was identified by correlating inserted white noise \underline{v} and input \underline{u} of the plant $\hat{\mathbf{P}}(j\omega)$ (Fig. 11). The frequency response of the plant can be reconstructed as follows:

$$\hat{\mathbf{P}}(j\omega) = \mathbf{C}^{-1}(j\omega) (\hat{\mathbf{S}}(j\omega) - \mathbf{I})^{-1} \quad (15)$$

which offers no problems as all matrices are 3×3 . Sensitivity matrix $\hat{\mathbf{S}}(j\omega)$ is constructed out of 3×3 responses of the system and $\mathbf{C}(j\omega)$ is diagonal matrix containing 3 SISO PI controllers. Bode magnitude plot of the frequency response of the identified plant $\hat{\mathbf{P}}(j\omega)$ for left, center and right position of the beam is shown on Fig. 12.

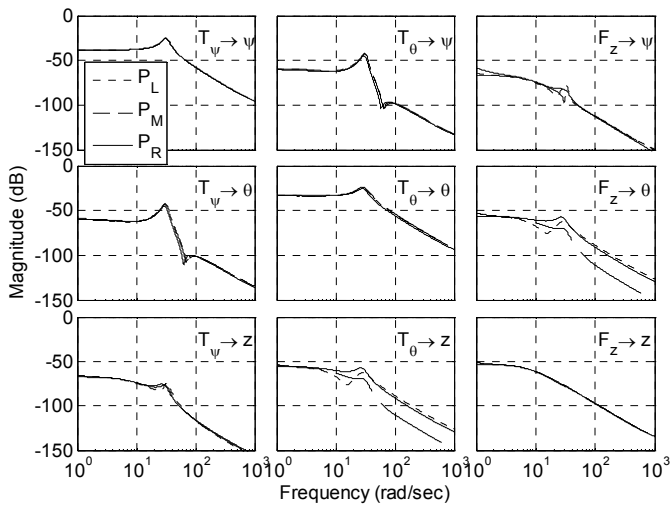


Fig. 10. Bode magnitude plot of the identified platform $\mathbf{P}_n = \mathbf{P}_6$ for 3 positions of the beam (P_{left} , P_{middle} , P_{right})

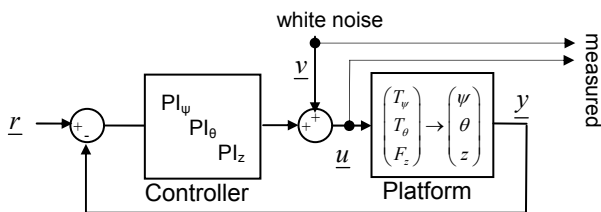


Fig. 11. The closed-loop system with applied white noise; measured with SigLab

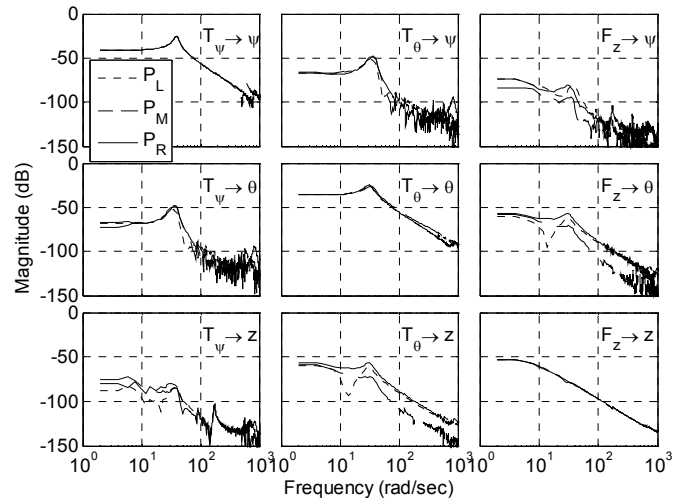


Fig. 12. Bode magnitude plot of $\hat{\mathbf{P}}(j\omega)$ identified with SigLab; 3 positions of the beam (P_{left} , P_{middle} , P_{right})

As you can see from the Fig. 10 and 12, the results obtained by both identification techniques are similar and the platform can be modeled with 6th-order MIMO model up to frequency of approx. 400 rad/s. The peaks in higher frequencies are caused by non-rigid modes and hysteresis in the bearings of the beam.

After the identification part, we have fine-tuned our LPV model described in previous chapter to match the results obtained by identification. Especially spring constants $k_{1,3}$ and damping d , which were estimated at first, had to be fine-tuned to match the identification. On Fig. 13 you can see the resulting bode magnitude plot of the model, which nicely fits with the identified transfer functions. In order to check whether indeed this LPV model fits closed-loop behavior, we have combined the model with the forces/torques applied on the platform due to the movement of the manipulator, as presented in Zurendonk, *et al.* (2007). We have used the same reference trajectory for the beam position x_b in the real

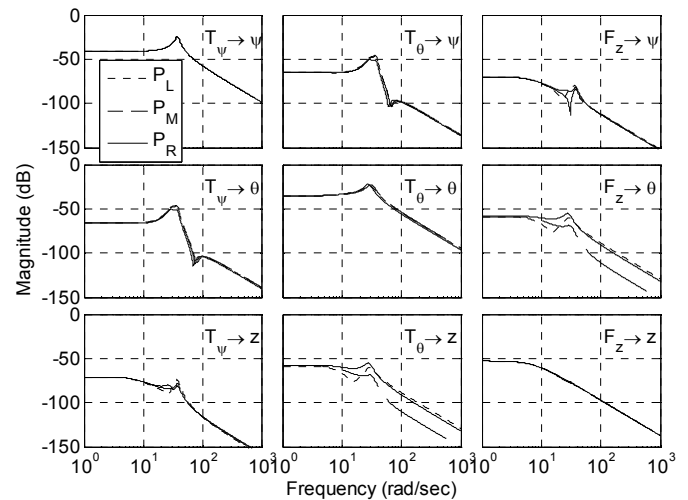


Fig. 13. Bode magnitude plot of the 6th order MIMO model of the platform based on (8) and (9); 3 positions of the beam

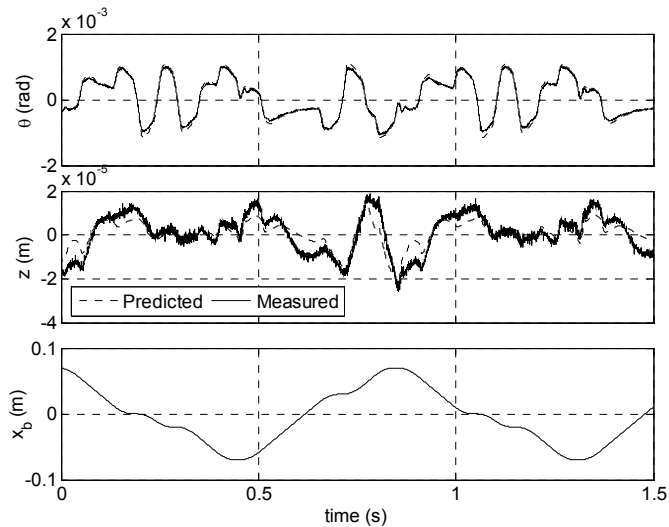


Fig. 14. Time plot of the platform perturbed by moving beam $x_b(t)$; predicted and measured values of $\theta(t)$ and $z(t)$

setup and in the model. The reference trajectory has been chosen is such way that the manipulator produces significant disturbances. From the predicted and measured values in Fig. 14, it can be seen that model prediction and measurement of the real setup match well. Actual position of the beam matches completely the reference trajectory because of well controlled manipulator.

6. CONCLUSIONS

Project and experimental setup of 3-DOF planar actuator with manipulator has been described in this paper. Our model of the 3-DOF planar actuator has been presented. Two identification techniques have been used to identify the system. Both techniques give us very close results. It has been verified that the experimental setup can be described by presented linear parameter-varying model. All obtained results will be used for further work which will deal with controller design for the identified system.

REFERENCES

Boeij, J. de, E. Lomonova, and A. Vandenput (2006). Contactless Energy Transfer to a Moving Load Part I&II. In: *Proc. IEEE Int. Symp. on Industrial Electronics*, pp. 739-750. Montreal, Canada.

Compter, J.C. (2004). Electro-dynamic planar motor. *Precision Engineering*, **Vol. 28**, pp. 171-180.

Gajdusek, M., J. de Boeij, A.A.H. Damen, P.P.J. v.d. Bosch (2007). Contactless planar actuator with manipulator - Experimental setup for control. In: *Proc. 6th Int. Symp. on Linear Drives for Industrial Applications*, pp. 57-58. Lille, France.

Gilson, M. and P.M.J. Van den Hof (2003). IV methods for closed-loop system identification. In: *13th IFAC Symposium on System Identification*, pp. 537-542. Rotterdam, The Netherlands.

Gustavsson, I., L. Ljung and T. Söderström (1977). Identification of processes in closed loop - identifiability and accuracy aspects. *Automatica*, **Vol. 13**, pp. 59-75.

Ho, B.J. and R.E. Kalman (1966). Effective construction of linear state-variable models from input-output functions. *Regelungstechnik*, **Vol. 14**, pp. 545-548.

Hof, P.M.J. Van den and R.J.P. Schrama (1993). An indirect method for transfer function estimation from closed loop data. *Automatica*, **Vol. 29**, pp. 1523-1527.

Hof, P.M.J. Van den, R.J.P. Schrama, O.H. Bosgra and R.A. de Callafon (1995). Identification of normalized coprime plant factors from closed-loop experimental data. *European J. Control*, **Vol. 1**, pp. 62-74.

Hof, P.M.J. Van den and R.A. de Callafon (1996). Multivariable closed-loop identification: from indirect identification to dual-Youla parameterization. In: *Proc. 35th IEEE Conference on Decision and Control*, pp. 1397-1402. Kobe, Japan.

Lierop, C.M.M. van, J.W. Jansen, A.A.H. Damen and P.P.J.v.d. Bosch (2006). Control of multi-degree-of-freedom planar actuators, In: *Proc. IEEE Int. Symp. on Control Applications*, pp. 2516-2521, Munich, Germany.

Ljung, L. (1993). Information content in identification data from closed-loop operation. In: *Proc. 32nd IEEE Conf. Decision and Control*, pp. 2248-2252. San Antonio, TX.

Ng, T.S., G.C. Goodwin, and B.D.O. Anderson (1977). Identifiability of MIMO linear dynamic systems operating in closed loop. *Automatica*, **Vol. 13**, pp. 477-485.

Oppenheim, A.V. and R.W. Schaffer (1999). *Discrete-time Signal Processing*, pp. 69-70, Prentice Hall, Upper Saddle River, NJ.

Schrama, R.J.P. (1992). *Approximate Identification and Control Design - with Application to a Mechanical System*. Dr. Dissertation, Delft Univ. Technology, The Netherlands.

Söderström, T., L. Ljung and I. Gustavsson (1976). Identifiability conditions for linear multivariable systems operating under feedback. *IEEE Trans. Automat. Contr.*, **Vol. 21**, pp. 837-840.

Söderström, T., P. Stoica and E. Trulsson (1987). Instrumental variable methods for closed-loop systems. In: *10th IFAC World Congress*, pp. 363-368. Munich, Germany.

Söderström, T. and P. Stoica (1989). *System Identification*. Prentice-Hall, Hemel Hempstead, U.K.

Ueda, Y. and H. Osaki (2007). Positioning characteristics of a coreless surface motor using halbach permanent magnet array. In: *Proc. Power Conversion Conf 2007*, pp. 614-621. Nagoya, Japan.

Vidyasagar, M. (1985). *Control System Synthesis - A Factorization Approach*. MIT Press, Cambridge, MA.

Zeiger, H.P. and J. McEwen (1974). Approximate linear realizations of given dimension via Ho's algorithm. *IEEE Trans. Automat. Contr.*, **Vol. 19**, pp. 153.

Zuurendonk, B., J. de Boeij, M. Steinbuch and E. Lomonova (2007). Modeling of Disturbance Forces of a x-y Manipulator on a Floating Platform. In: *Proc. 6th Int. Symp. on Linear Drives for Industrial Applications*, pp. 61-62. Lille, France.